MINOR HEAD LOSS ANALYSIS OF LAMINAR FLUID FLOW IN COMPLEX GEOMETRIES

Manh Hung Nguyen[1], Truong Sang Ha[1,*]

[1]*Faculty of Mechanical Engineering, Le Quy Don Technical University, Hanoi, Vietnam*

Abstract

Minor head loss occurs in most hydraulic equipment because the flow is affected by a shape change. Head loss analysis is essential in designing and fabricating hydraulic equipment and systems. In the general case, the evaluation of head losses is challenging and usually done by experimental methods. Recently, the calculation has been more convenient using the computational fluid dynamics (CFD) method. This article employs the finite element method (FEM) to evaluate the local hydraulic losses in complex geometries discretized by unstructured mesh. The method is applied to the laminar flow of Newtonian fluid. First, the code is validated by comparing the numerical solution with experimental data and previous numerical results. The code is then employed to simulate different problems, including a complex geometry that mimics the control valve in hydraulic systems. Simultaneously, the minor loss coefficient is calculated for different Re numbers. From the results, the minor loss coefficient is large for low Re, and can be up to 700 for Re = 10 of complicated geometry. For a high Re, the minor loss coefficient is rapidly decreased and close to the value of a turbulent model.

Keywords: *Minor head loss; laminar flow; complex geometries; FEM; CFD.*

1. Introduction

Hydraulic loss occurs in much equipment in the hydraulic system because of the viscosity of the liquid or a change in geometry in the flow direction. Recently, head loss has become the main concern in the design and fabrication of hydraulic equipment and systems since it directly affects the efficiency of the machines. Head loss analysis has an essential role and can be found in many fields in industrial design, such as efficiency improvement of the gearbox [1], improvement of the stability and lifespan of rotating components in a centrifugal pump [2] or investigation of the performance of orifice meter devices [3, 4].

In the general case, evaluating head losses is difficult and time-consuming. Previous studies of minor head losses are usually done by experimental methods [5, 6]. The experimental study has a disadvantage in limiting a deeper understanding of the

[*] Email: sanght.st@lqdtu.edu.vn
DOI: 10.56651/lqdtu.jst.v18.n03.728

physical phenomena in fluid flow. Recently, thanks to the improvement of computer hardware, numerical calculation has become more convenient using the computational fluid dynamics (CFD) method. The local hydraulic resistances and the character of the fluid flow in the pipelines are described in detail using the finite volume method by Chemezov [7]. Fluid flows through a sudden contraction, and the minor loss coefficient is numerically calculated using the ANSYS program [8].

With the development of numerical method, the CFD method is more and more common for the analysis of head loss problems in designing machines. This article employs the finite element method (FEM) to calculate laminar fluid flow and evaluate the minor head losses in complex geometries based on unstructured meshes. The FEM is one of the most common approaches based on the grid method to solve the effect of the Reynolds (Re) number on the minor loss coefficient is also investigated. Using the concept of shape functions, FEM can work well on any type of mesh or boundary condition. The rest of the article is constructed as follows: Section 2 briefly describes the numerical method for solving fluid flow dynamics. Some benchmark problems for evaluating minor head loss are shown in Section 3, and the conclusions are drawn in Section 4.

2. Methodology

2.1. Governing equations

The fluid flow is assumed as an incompressible flow of a Newtonian fluid, the governing equations are the incompressible Navier-Stokes equations which can be written as follows in the Eulerian framework [9]:

$$\begin{aligned} &\nabla \cdot \mathbf{u} = 0 \quad \text{in } \Omega && \text{(a)} \\ &\rho\left[\frac{\partial \mathbf{u}}{\partial t} + \mathbf{u}\cdot\nabla\mathbf{u}\right] = \nabla\cdot\boldsymbol{\sigma} \quad \text{in } \Omega && \text{(b)} \end{aligned} \tag{1}$$

where $\rho, \mathbf{u}, \boldsymbol{\sigma}$ and Ω are the fluid density, the fluid velocity, the fluid stress tensor, and the fluid domain, respectively.

The fluid domain's boundary is denoted by Γ. The corresponding constitutive equations for fluid flow in Eq. (1) are written as follows [10]:

$$\begin{aligned} &\boldsymbol{\sigma} = -p\mathbf{I} + \boldsymbol{\tau}, && \text{(a)} \\ &\boldsymbol{\tau} = \mu[\nabla\mathbf{u} + (\nabla\mathbf{u})^{\mathrm{T}}] && \text{(b)} \end{aligned} \tag{2}$$

where $p, \mu, \boldsymbol{\tau}$, and $\mathbf{I}$ indicate the pressure, the dynamic fluid viscosity, the shear stress tensor, and the second-order identity tensor, respectively.

The boundary conditions are described as follows:

$$\begin{aligned} &\mathbf{u} = \bar{\mathbf{u}} \quad \text{on } \Gamma_{\mathbf{u}}, && \text{(a)} \\ &\boldsymbol{\sigma} \cdot \mathbf{n} = \bar{\mathbf{t}} \quad \text{on } \Gamma_{\mathbf{t}} && \text{(b)} \end{aligned} \tag{3}$$

where **n** denotes the outward unit normal vector to the fluid boundary. $\Gamma_{\mathbf{u}}$ and $\Gamma_{\mathbf{t}}$ are the boundaries where the velocity $\bar{\mathbf{u}}$ and traction $\bar{\mathbf{t}}$ are imposed on the Dirichlet and Neumann boundary conditions, respectively.

2.2. Finite element method for incompressible fluid flow

FEM is a popular approach to computational mechanics, especially to solve thermal conduction, the Poisson equation or the Navier-Stokes equation. It is also constructive for unstructured meshes from a complex geometric domain. This study employs the fractional method [11] to solve the incompressible Navier-Stokes equations. The second-order-implicit Crank-Nicolson scheme is used for the temporal discretization of the diffusion terms and the second-order-explicit Adams-Bashforth scheme for the convective terms. In this approach, the intermediate velocity $\hat{u}$ is solved by the momentum equation. Then, the pressure is obtained by solving the Poisson equation, and the velocity is corrected by the pressure in the last step.

We use the *P2P1* finite element, as shown in Fig. 1. The pressure is placed at the vertices while the velocity is placed on both vertices and middle points. The momentum equations are discretized using a consistent streamline upwind Petrov-Galerkin method and the pressure equation using a Galerkin method, and their weak formulation can be written as follows [11]:

Find $u \in H^1(\Omega)$, $\hat{u} \in H^1(\Omega)$ and $p \in H^1(\Omega)$ such that:

$$\begin{aligned} &\int_\Omega w_i \frac{\hat{u}_i - u_i^n}{\Delta t} d\Omega + \frac{\mu}{2\rho} \int_\Omega w_{i,j} \hat{u}_{i,j} d\Omega = \frac{\mu}{\rho} \int_{\Gamma_p} w_i \bar{t}_i^u \, d\Gamma - \\ &\quad - \frac{\mu}{2\rho} \int_\Omega w_{i,j} u_{i,j}^n d\Omega - \frac{1}{2} \int_\Omega w_i \left(3u_j^n u_{i,j}^n - u_j^{n-1} u_{i,j}^{n-1} \right) d\Omega \end{aligned} \tag{4}$$

$$\int_\Omega q_{,i} \, p_{,i}^{n+1} d\Omega = \int_{\Gamma_t} q \, p_{,i}^{n+1} n_i d\Gamma - \frac{\rho}{\Delta t} \int_\Omega q \hat{u}_{i,i} d\Omega \tag{5}$$

$$\int_\Omega w_i \frac{u_i^{n+1} - \hat{u}_i}{\Delta t} d\Omega = -\frac{1}{\rho} \int_\Omega w_i p_{,i}^{n+1} d\Omega \tag{6}$$

for all admissible functions $w \in V$, $q \in P$ where $V = \{w \mid w \in H^1(\Omega),\ w = 0 \ \text{ on } \Gamma_u\}$, $P = \{q \mid q \in H^1(\Omega),\ q = 0 \ \text{ on } \Gamma_p\}$, $H^1(\Omega)$ denotes the Sobolev space defined on the spatial domain Ω. In Eq. (4), $\bar{t}_i^u = u_{i,j} n_j$ denotes the Neumann boundary of velocity. It should be noted that Eq. (5) is the Poison-type equation.

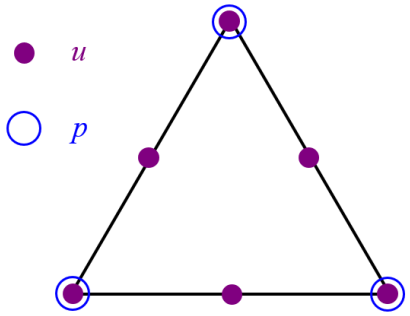

Fig. 1. Degrees of freedom assigned for the P2P1 on the triangular finite element.

2.3. Evaluation of the minor loss coefficient

The energy equation for incompressible fluid flow in a horizontal pipe is usually written as (the body force is neglected) [8]:

$$\left(\frac{p_1}{\gamma} + \alpha_1 \frac{v_1^2}{2g}\right) - \left(\frac{p_2}{\gamma} + \alpha_2 \frac{v_2^2}{2g}\right) = h_l + h_c \tag{7}$$

where γ is the fluid specific weight; h_l and h_c are the major and minor energy loss per unit mass; p_1 and p_2 are the averaged static pressures over the entire cross-section; v_1 and v_2 are the average velocities; α_1 and α_2 are the kinetic energy correction factors at the upstream and downstream sections, respectively.

In this work, we only focus on the minor losses encountered across fittings, bends, or abrupt area changes that occur primarily because of flow separation. In this case, the major loss h_l is small and can be neglected. The minor losses h_c are usually expressed in terms of a loss coefficient ξ where $h_c = \xi \frac{v_1^2}{2g}$. From Eq. (7), the minor loss coefficient can be calculated by:

$$\xi = \frac{\left(\frac{p_1}{\rho} + \alpha_1 \frac{v_1^2}{2}\right) - \left(\frac{p_2}{\rho} + \alpha_2 \frac{v_2^2}{2}\right)}{\frac{v_1^2}{2}} \tag{8}$$

For a simple case such as the sudden expansion of the pipeline, ξ only depends on the area of sections [12]:

$$\xi = \left(1 - \frac{A_1}{A_2}\right)^2 \tag{9}$$

where A_1 and A_2 are the cross-sectional areas at the upstream and downstream sections, respectively.

To determine the major loss, we use the two sections (upstream and downstream) that are close to the minor loss area. It means that the flow at the two sections may not be fully developed, and therefore, factors α_1 and α_2 on Eq. (7) are less than 2. We can calculate the factors by following the equation [12]:

$$\alpha = \frac{\int_A u^3 dA}{v^3 A} \tag{10}$$

3. Results and discussions

In this section, some fluid flow problems are simulated using the finite element method described in Section 2.2. First, the code is validated by comparing the results obtained from the present code with the experimental data. Then, the code is used to calculate the minor loss coefficient for the complex geometry case.

3.1. Validation code

Firstly, the present code is validated by comparing the simulation results with the data from experimental research. A pulsatile flow through stenosis tubes described in [13] is employed. The geometry and boundary conditions are shown in Fig. 2. A pulsatile flow is applied at the inlet, as shown in Fig. 3, and a zero pressure is set at the outlet. The non-slip condition is applied to the wall. Because of symmetric, we only simulate the problem in the cylindrical coordinates, and a half domain is selected. The grid shown in Fig. 4 is used for the grid independent test. A high resolution is located in the stenosis region. Table 1 shows the information of four resolutions of grid data from coarse to very fine mesh. For validation code, we use a velocity at a point on the center line. Fig. 5 compares the results obtained from different resolutions at a point $z_0 = 2.5D$. It can be seen that the results from grid-3 (fine grid) are identical to those from grid-4, so the grid-3 is selected for this validation. Fig. 6 shows the streamline and velocity magnitude of fluid flow at the instant time in the stenosis

region. Velocities at points $z_1 = 1D$ and $z_2 = 4.3D$ are shown in Fig. 7. It can be found that the results from the present code are in good agreement with the experimental data of Ojha [13] and the previous numerical solution of Hun [14] and Banerjee [15].

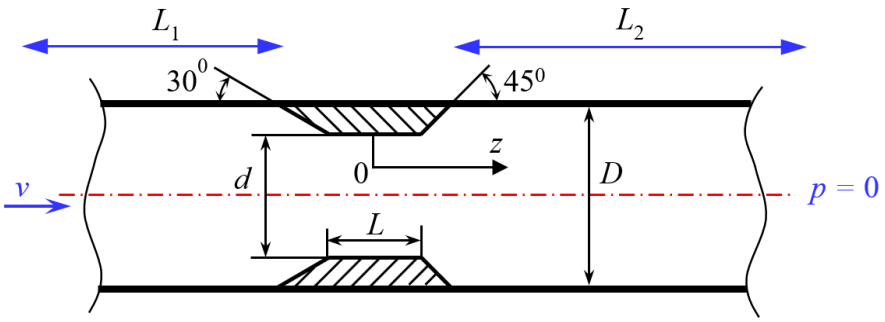

Fig. 2. Geometry and boundary conditions for validation problem.

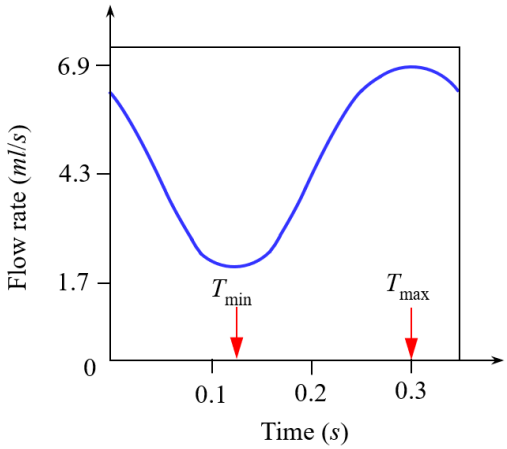

Fig. 3. Pulsatile flow at the inlet [13].

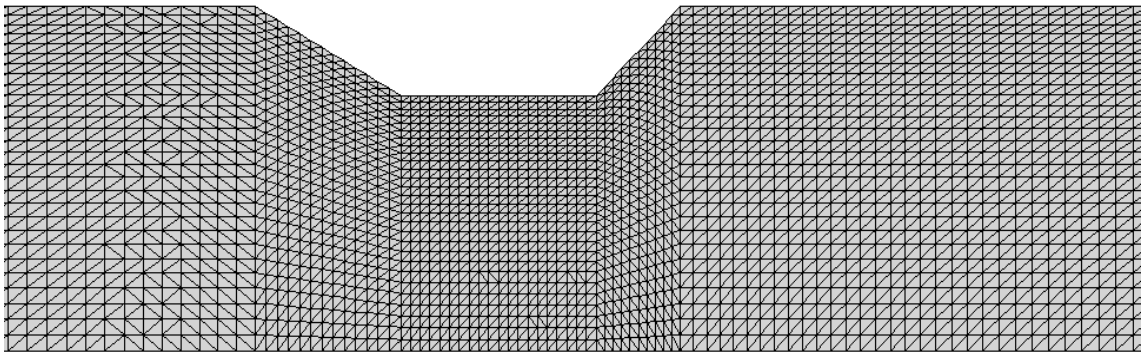

Fig. 4. Unstructured grid used for simulation (coarse grid).

Table 1. Resolutions for mesh independent test

Grid resolutions	**nx**	**ny**	**Total nodes**
Grid 1 (coarse)	575	29	16,675
Grid 2 (medium)	827	41	33,907
Grid 3 (fine)	1,171	57	66,747
Grid 4 (very fine)	1,499	79	118,421

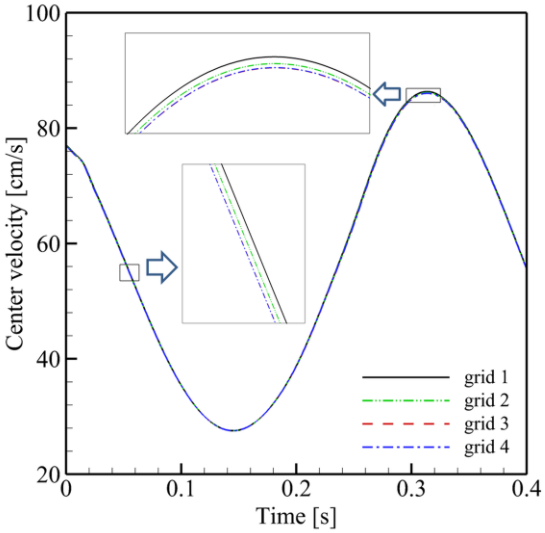

Fig. 5. Grid independent test: Comparison of velocity at z_0 = 2.5D on center line.

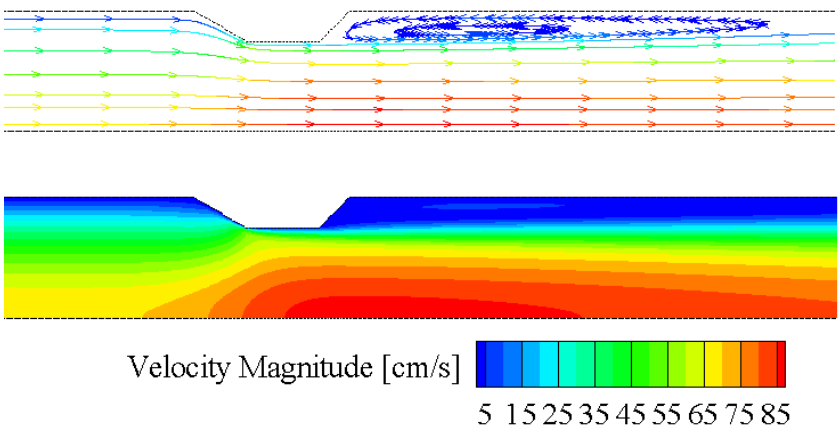

Fig. 6. Streamline and velocity magnitude at time = 0.032 [s].

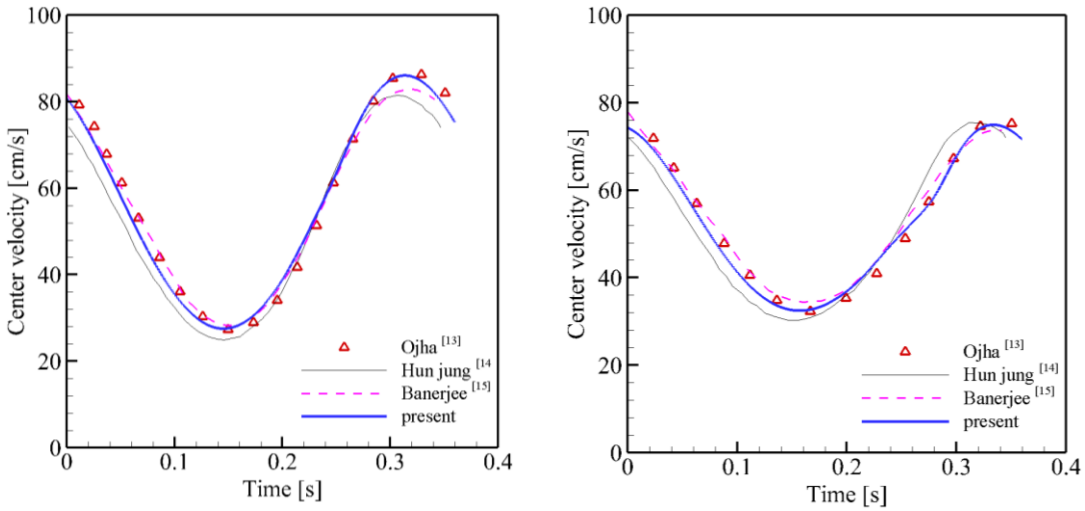

Fig. 7. Center velocity: Comparison of present results with other authors.

3.2. Flow in the sudden expansion channel

The first simulation problem is a fluid flow in the sudden expansion 2D channel, in which the geometry and boundary conditions are given in Fig. 8. The channel width is D = 0.1 m, a constant velocity of fluid flow u_{in} = 0.1 m/s is set at the inlet, and a zero pressure is set at the outlet. The density and viscosity of fluid flow are set by ρ = 1000 kg/m^3 and μ = 0.1 Pa.s, and the Re number is calculated at the inlet is 100. A high-resolution grid is shown in Fig. 9, with the number of nodes and elements being 16,505 and 8,112, respectively. The simulation is performed with a time step Δt = 0.005 s. The solution is steady, and the velocity field is shown in Fig. 10. It can be seen that vortices appear after the expansion of the channel, and the local loss is created in this region. Because of the sudden expansion, the pressure is significantly reduced at the expansion section, as shown in Fig. 11 with the variant Re number by changing velocity at the inlet. Table 2 illustrates the minor loss coefficient obtained by numerical solution. It shows that it decreases when increasing the Re number. In the case of Re = 100, the numerical solution (0.38) agrees well with the results from Eq. (9) for the turbulent case (0.36).

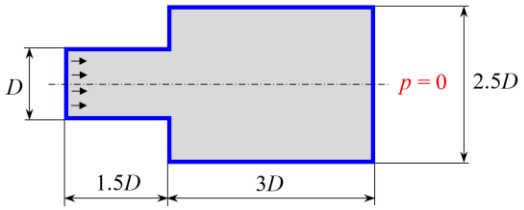

Fig. 8. Geometry and boundary condition of a sudden expansion problem.

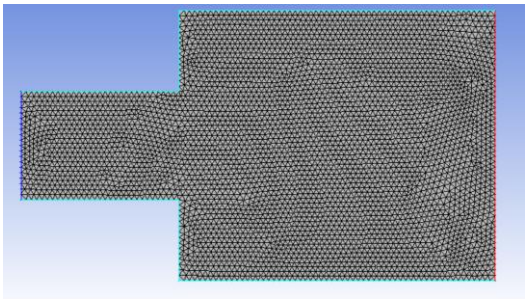

Fig. 9. Grid of a sudden expansion problem.

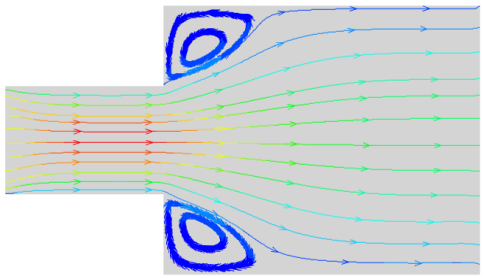

Fig. 10. Velocity field (Re = 20).

Table 2. The minor loss coefficient obtained by numerical solution

Re	**10**	**20**	**50**	**100**
ξ	1.10	0.71	0.48	0.38

3.3. Flow in a 90-degree bend 2D

The second problem is a fluid flow in the 90-degree bend 2D (elbow), which the geometry and boundary conditions are given in Fig. 12a. The width and the radius of the bend are D = 1.0 m and R = 1.0 m. The fluid flow velocity at the inlet is set by u_{in} = 0.1 m/s, and a zero pressure is set at the outlet. The density and viscosity of fluid flow are set by ρ = 100 kg/m^3 and μ = 0.1 Pa.s, and the Re number is calculated at the inlet is 100. The grid is shown in Fig. 12b, with the number of nodes and elements being 11,275 and 5,494, respectively. The simulation is performed with a time step Δt = 0.01 s. A steady solution is obtained, and the velocity field and pressure contours are shown in Fig. 13. When the Re number increases tenfold, vortices appear behind the inner wall of the bend (Fig. 13b). This phenomenon can be found in many experimental data because of the line separation effect. These vortices are also increasing the local loss of fluid flow. Table 3 illustrates the minor loss coefficient obtained by numerical solution. Similar to the problem in Section 3.2, the coefficient decreases when the Re number increases.

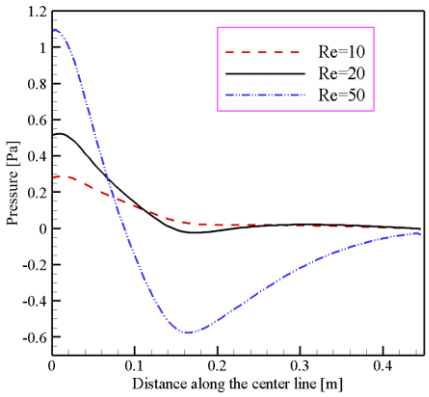

Fig. 11. Pressure along the center line.

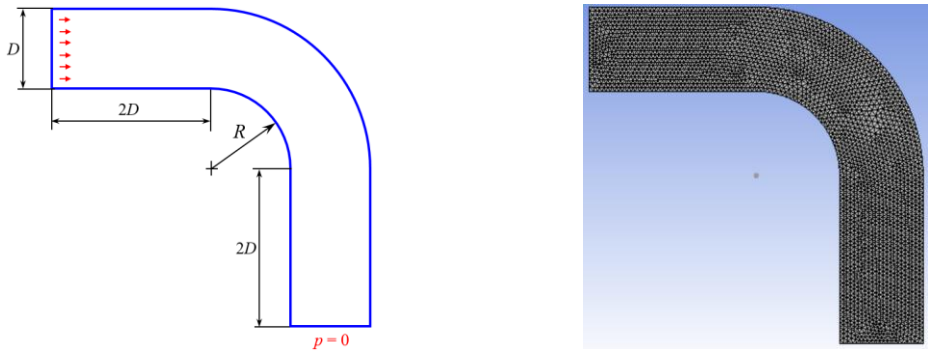

a) Geometry and boundary condition b) P2P1 grid

Fig. 12. Geometry and grid used in the simulation.

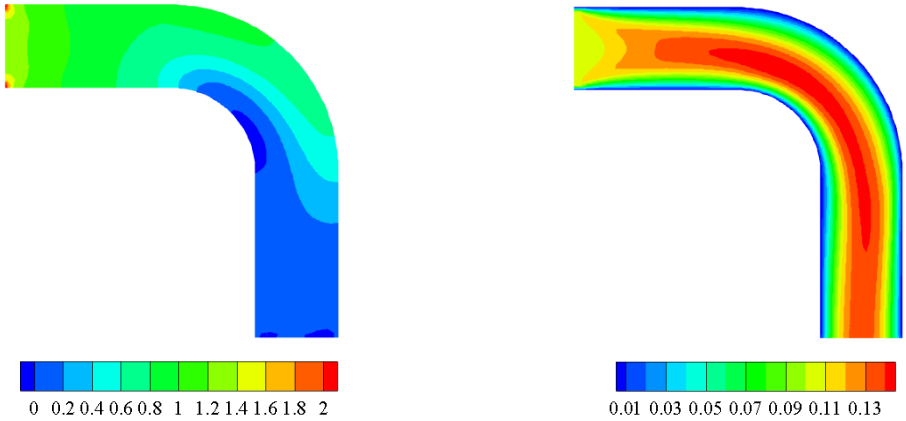

a) Re = 100

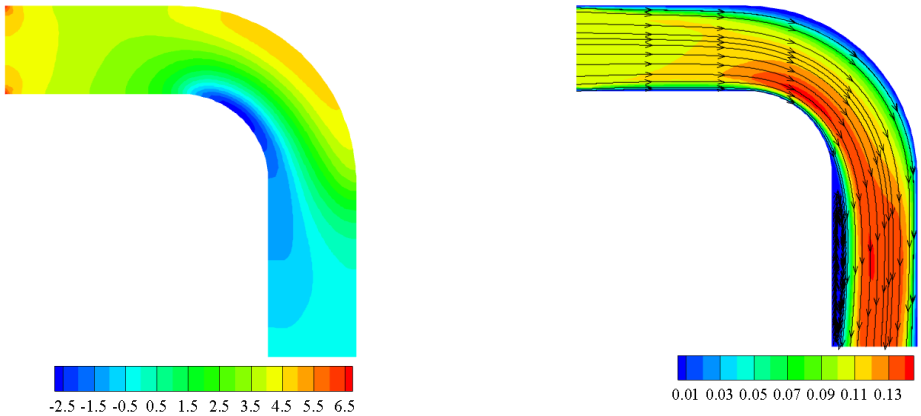

b) Re = 1000

Fig. 13. Pressure and magnitude of velocity (left: pressure [Pa], right: velocity [m/s]).

Table 3. The minor loss coefficient obtained by numerical solution

Re	**10**	**100**	**1000**
ξ	14.0	2.0	0.3

3.4. Flow in a complex geometry

Finally, a complex geometry found in some hydraulic system control valve components is adopted. Fig. 14 shows the geometry of the simulation problem, and the unstructured grid is shown in Fig. 15, with the number of nodes and elements being 16,932 and 8,136. The boundary condition and physical property of the fluid are similar to those in Section 3.2. The problem is tested with Re of 10, 20, 50, and 100. Fig. 16 illustrates the pressure field and streamlines for Re = 50. The pressure drop, in this case, is much larger than in the case of the sudden expansion problem in Section 3.2 because the flow is affected by the central obstruction. In addition, many flow vortices near the obstruction lead to the high energy loss of the flow. Therefore, the minor loss coefficient of this problem is very high, as shown in Tab. 4.

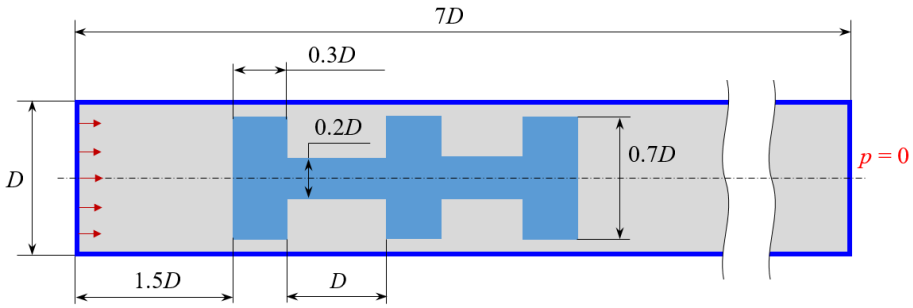

Fig. 14. Geometry and boundary condition of a complex geometry.

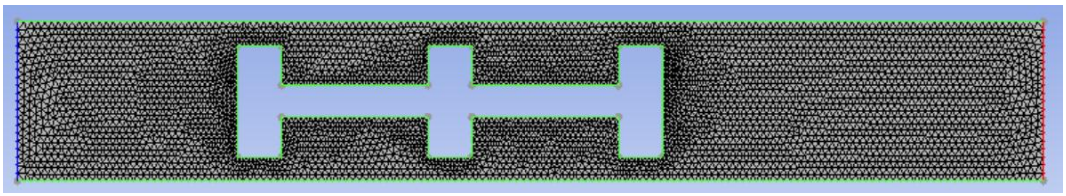

Fig. 15. Grid of a complex geometry.

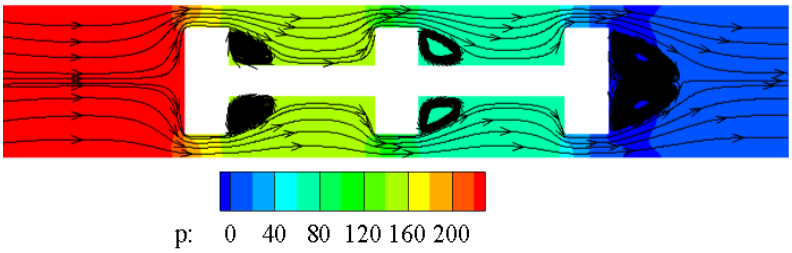

Fig. 16. Pressure field and streamline (Re = 50).

Table 4. The minor loss coefficient of the complex geometry

Re	**10**	**20**	**50**	**100**
ξ	719	369	159	96

Similar to the sudden expansion problem, the minor loss coefficient decreases with increasing Re. Based on these values, an estimation of the minor loss coefficient with variant Re numbers is shown in Fig. 17. Therefore, in this problem, the coefficient is approximated by the following Eq. (11):

$$\xi = \frac{5280}{\mathrm{Re}^{0.881}} \tag{11}$$

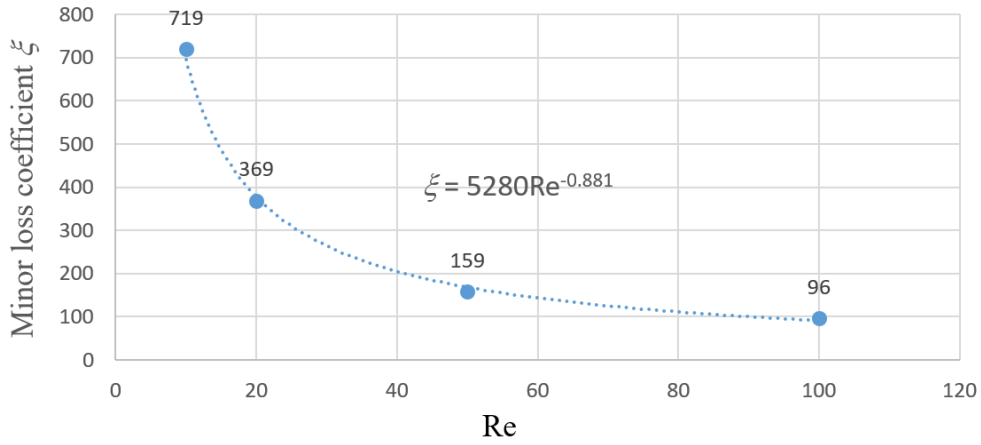

Fig. 17. Estimation of the minor loss coefficient with variant Re numbers.

This approximation can be used for other cases of different Re numbers without a simulation procedure.

4. Conclusion

The FEM is employed in this article to evaluate the local hydraulic losses in complex geometries on unstructured meshes. The method is applied to laminar flow of a Newtonian fluid. The code is validated by comparing the numerical solution with experimental data and previous works. The code is then employed to simulate various geometries, including a complex shape that mimics the control valve in hydraulic systems. Based on that, the minor loss coefficient is calculated according to different Re numbers.

From some benchmark problems, the conclusions are drawn as follows:

- In general, the minor head loss is dependent on many factors that are hard to evaluate by analysis. Therefore, the numerical method is robust and effective for

calculating hydraulic problems.

- The appearance of vortices in the complex geometry increases with the increasing of Re number which leads to an enormous hydraulic loss in fluid flow.

- The minor loss coefficient value decreases as the Re numbers increase for a particular geometry case in the laminar flow.

The study has an important role in calculating the local loss of fluid flow in machine equipment. Therefore, it can be helpfully used for conducting the hydraulic system in the industry. The present code is a very effective tool for evaluating the local loss because it can work in any complex geometry. Benchmark cases in this work are 2D space (including the 3D axis symmetry case); the extension to 3D space with the tetrahedron element is straightforward and will be reported in future work.

References

[1] C. Gorla, F. Concli, K. Stahl, B. R. Höhn, K. Michaelis, H. Schultheiß, and J. P. Stemplinger, "Hydraulic losses of a gearbox: CFD analysis and experiments", *Tribology International*, Vol. 66, pp. 337-344, 2013. DOI: 10.1016/j.triboint.2013.06.005

[2] M. Guo, S. H. Liu, X. L. Tang, Z. G. Zuo, and X. Q. Li, "Evaluation of shaft forces in a vertical canned motor through local hydraulic loss analysis", *Advances in Mechanical Engineering*, Vol. 10(3), 2018. DOI: 10.1177/168781401876559

[3] H. M. Abd, O. R. Alomar, and I. A. Mohamed, "Effects of varying orifice diameter and Reynolds number on discharge coefficient and wall pressure", *Flow Measurement and Instrumentation*, Vol. 65, pp. 219-226, 2019. DOI: 10.1016/j.flowmeasinst.2019.01.004

[4] H. S. Sondh, S. N. Singh, V. Seshadri, and B. K. Gandhi, "Design and development of variable area orifice meter", *Flow Measurement and Instrumentation*, Vol. 13, Iss. 3, pp. 69-73, 2002. DOI: 10.1016/S0955-5986(02)00030-4

[5] P. H. Dawson, "Windage Loss in Larger, High-Speed Gears", *Proceedings of the Institution of Mechanical Engineers, Part A: Power and Process Engineering*, Vol. 198, Iss. 1, pp. 51-59, 1984. DOI: 10.1243/PIME_PROC_1984_198_007_02

[6] S. Seetharaman, A. Kahraman, M. D. Moorhead, and T. T. Petry-Johnson, "Oil Churning Power Losses of a Gear Pair: Experiments and Model Validation", *Journal of Tribology*, Vol. 131, Iss. 2, 2009, 022202. DOI:10.1115/1.3085942

[7] D. Chemezov, "The character of the fluid flow in the pipelines with the local hydraulic resistances", *ISJ Theoretical & Applied Science*, Vol. 44, Iss. 12, pp. 62-68, 2016. DOI:10.15863/TAS.2016.12.44.13

[8] J. Weber, G. N. Facas, M. Horst, and M. Sharobeam, "Using FLUENT to Supplement Theory in an Introductory Fluid Mechanics Course", *International Journal of Hydraulic Engineering*, Vol. 8, No. 1, pp. 11-21, 2019. DOI: 10.5923/j.ijhe.20190801.03

[9] S. T. Ha, T. D. Nguyen, V. C. Vu, M. H. Nguyen, and M. H. Nguyen, "A study of fluid-structure interaction of unsteady flow in the blood vessel using finite element method", *Modern Mechanics and Applications (Select Proceedings of ICOMMA 2020)*, 2021, pp. 1089-1101. DOI:10.1007/978-981-16-3239-6_85

[10] S. T. Ha, V. C. Vu, M. H. Nguyen, and M. D. Nguyen, "Numerical simulation for fluid-structure interaction of a blood flow with the aortic valve using the fem monolithic formulation", *Journal of Science and Technique*, Vol. 16, No. 03, pp. 49-60, 2021. DOI: 10.56651/lqdtu.jst.v16.n03.277

[11] M. H. Nguyen, S. T. Ha, and V. D. Le, "Numerical simulation of 2D fluid flow using the finite element discretization on unstructured grid combined with adaptive mesh refinement technique", *Journal of Science and Technology* (Hanoi University of Industry), Vol. 57-special, pp. 84-90, 2021.

[12] P. J. Pritchard and J. W. Mitchell, *Introduction to Fluid Mechanics*, 9th ed., Wiley, 2015.

[13] M. Ojha, R. S. C. Cobbold, K. W. Johnston, and R. L. Hummel, "Pulsatile flow through constricted tubes: An experimental investigation using photochromic tracer methods", *Journal of Fluid Mechanics*, Vol. 203, pp. 173-197, 1989. DOI: 10.1017/S0022112089001424

[14] J. Hun, J. W. Park, and C. G. Park, "Asymmetric flows of non-Newtonian fluids in symmetric stenosed artery", *Korea-Australia Rheology Journal*, Vol. 16, No. 2, pp. 101-108, 2004.

[15] M. K. Banerjee, R. Ganguly, and A. Datta, "Effect of pulsatile flow waveform and Womersley number on the flow in stenosed arterial geometry", *International Scholarly Research Network*, 2012. DOI: 10.5402/2012/853056

PHÂN TÍCH TỔN THẤT THỦY LỰC CỤC BỘ TRONG DÒNG CHẢY TẦNG TẠI CÁC KẾT CẤU PHỨC TẠP

Nguyễn Mạnh Hùng[a], Hà Trường Sang[a]

[a]*Khoa Cơ khí, Trường Đại học Kỹ thuật Lê Quý Đôn*

Tóm tắt: Tổn thất thủy lực cục bộ xảy ra trong hầu hết các thiết bị thủy lực do dòng chảy bị ảnh hưởng bởi việc thay đổi hình dạng. Việc phân tích tổn thất thủy lực có ý nghĩa quan trọng trong thiết kế và chế tạo các thiết bị và hệ thống thủy lực. Trong trường hợp tổng quát, việc phân tích này rất khó khăn và thường được thực hiện theo phương pháp thực nghiệm. Gần đây, việc tính toán thuận tiện hơn nhờ phương pháp CFD. Trong bài báo này, phương pháp phần tử hữu hạn được sử dụng để tính toán tổn thất thủy lực cục bộ trong các kết cấu phức tạp dựa trên lưới không cấu trúc. Phương pháp này được thực hiện cho dòng chảy tầng chất lỏng Newton. Trước tiên, thuật toán được kiểm chứng qua việc so sánh lời giải số với các dữ liệu thực nghiệm và kết quả số trước đó. Sau đó, thuật toán này được sử dụng để mô phỏng các bài toán khác nhau, bao gồm cả dạng hình học phức tạp tương tự van điều khiển trong các hệ thống thủy lực. Đồng thời, hệ số hiệu chỉnh động năng được tính theo các số Re khác nhau. Dựa vào kết quả phân tích, hệ số tổn thất cục bộ đạt giá trị lớn đối với số Re thấp, có thể lên đến 700 đối với Re = 10 đối với hình học phức tạp. Đối với số Re cao, hệ số tổn thất cục bộ được giảm xuống nhanh và gần tiệm cận với giá trị của dòng chảy rối.

Từ khóa: *Tổn thất thủy lực cục bộ; dòng chảy tầng; kết cấu hình học phức tạp; FEM; CFD.*

Received: 26/11/2021; Revised: 25/07/2022; Accepted for publication: 11/11/2022

❑